ELSEVIER

www.elsevier.nl/locate/jorganchem

Journal of Organometallic Chemistry 582 (1999) 319–327

Journal of Organometallic Chemistry

Synthesis, characterization and X-ray structural, electrochemical and Mössbauer study of mercury(II) complexes with 1′-(diphenylphosphino)ferrocenecarboxylic acid

Petr Štěpnička [a,*], Ivana Císařová [a], Jaroslav Podlaha [a], Jiří Ludvík [b], Martin Nejezchleba [c]

[a] *Department of Inorganic Chemistry, Charles University, Hlavova 2030, 128 40 Prague 2, Czech Republic*
[b] *J. Heyrovský Institute of Physical Chemistry, Academy of Sciences of the Czech Republic, 182 23 Prague 8, Czech Republic*
[c] *Laboratory of Mössbauer Spectroscopy, Charles University, 182 00 Prague 8, Czech Republic*

Received 8 October 1998; received in revised form 23 December 1998

Abstract

Reaction of mercury(II) halides with 1′-(diphenylphosphino)ferrocenecarboxylic acid (Hdpf) affords $[HgX_2(Hdpf\text{-}P)_2]$ or $[HgX(\mu\text{-}X)(Hdpf\text{-}P)]_2$ complexes (X = Cl, Br, I) depending on the stoichiometry of the educts. The complexes have been studied by IR, Mössbauer and solution NMR spectroscopy. In dimethyl sulfoxide-d_6 solution, ^{1}H- and ^{31}P{^{1}H}-NMR spectra indicate solvolytic cleavage of the mercury(II)–phosphine bond resulting in a partial decomplexation of the phosphine ligand. Electrochemical measurements in donor solvents also confirm the presence of the non-coordinated ligand since the electrochemical behavior is the superposition of that of the product of solvolysis and of the ligand. X-ray structural analysis, of the representatives of both types, was carried out: $[HgBr_2(Hdpf\text{-}P)_2]$ ($[C_{46}H_{38}Br_2Fe_2HgO_4P_2]$, monoclinic; space group $C2/c$, $a = 19.453(1)$, $b = 13.704(1)$, $c = 17.929(2)$ Å; $\beta = 114.953(7)°$; $Z = 4$) and $[HgBr(\mu\text{-}Br)(Hdpf\text{-}P)]_2 \cdot 2CH_3CO_2H$ ($[C_{54}H_{54}Br_4Fe_2Hg_2O_{12}P_2]$, triclinic; space group $P\bar{1}$, $a = 9.442(1)$, $b = 11.7101(9)$, $c = 14.806(1)$ Å; $\alpha = 109.692(7)$, $\beta = 92.494(9)$, $\gamma = 101.883(7)°$; $Z = 1$). The *P*-monodentate coordination of the phosphinocarboxylic ligand was confirmed in both cases, the carboxyl group being involved in hydrogen bonding to carboxyl groups of either neighboring ligand or solvating acetic acid. The expected Br_2P_2 and Br_3P tetrahedral donor sets around Hg(II) are the subject of different degrees of deformation due to steric effects. ^{57}Fe Mössbauer spectra of the complexes also point to the simple *P*-coordination of the ferrocenylphosphino ligand, as follows from the decrease of the quadrupole splitting and only a slight variation of the isomer shift on going from ligand to complex.

Keywords: Ferrocene; Mercury; Hybrid phosphines; X-ray structure; Electrochemistry; Mössbauer spectroscopy

1. Introduction

Ligands which are capable of linking two or more metal centers to form multinuclear complexes play an important role in coordination chemistry because of potential applications of these complexes as homogeneous catalysts, materials with specific magnetic and conducting properties [1] and/or precursors for metal-rich polymers [2]. One of straightforward synthetic routes leading to these compounds is offered by metal-containing ligands, mainly organometallic. This field is dominated by ferrocene-based ligands—not only for their structural versatility but also for the possibility of monitoring electron-transfer induced structural and electronic changes in their coordination compounds by following the redox properties of the ferrocene framework [3,4]. In contrast to numerous papers dealing with the coordinaton chemistry of various *P*; *P*,*P*′ and *P*,*N*-ferrocene donors, only a small amount work has been done on the description of complexes with ferrocene *O*,*P*-donors although ferrocene-based phosphinoethers [5], phosphinoamides [6], phosphinoesters [7] and phosphinoaldehydes [8,9] (i.e. potential ligands) were reported. The complexes of β-ketophosphine $Ph_2PCH_2C(O)Fc$ (Fc = ferrocenyl) with Ni [10,11] and

* Corresponding author.
E-mail address: stepnic@natur.cuni.cz (P. Štěpnička)

0022-328X/99/$ - see front matter
PII: S0022-328X(99)00071-6

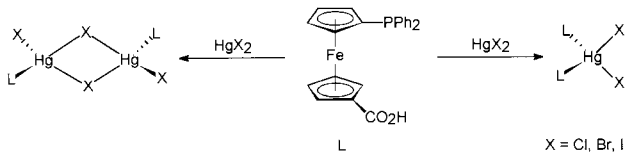

Scheme 1.

Pd [12] may serve as rather rare examples of coordinated donors of that type.

Recently, we have reported on the synthesis and properties of the novel ferrocene-based phosphinocarboxylic ligand, 1′-(diphenylphosphino)ferrocenecarboxylic acid (Hdpf) [13] and its complexes with Pd(II) and Pt(II) [14], Cu(I) [15], and Ru(II) [4] all of which contain the ligand as the *P*-donor. We have also described the synthesis and characterization of several Rh(I) complexes in which the deprotonated form of the ligand, dpf^-, acts as the *cis*-*O*,*P*-chelating donor [16]. Herein we present the syntheses and the X-ray structural, spectral and electrochemical investigation of mercury(II) complexes of the title ligand.

2. Results and discussion

2.1. Syntheses and characterization

The complexes $[HgX_2(Hdpf\text{-}P)_2]$ (X = Cl, Br, I; **1a**–**c**) and $[HgX(\mu\text{-}X)(Hdpf\text{-}P)]_2$ (**2a**–**c**) were synthesized in yields exceeding 90% by the reaction of stoichiometric amounts of the phosphinocarboxylic ligand Hdpf and the appropriate mercury(II) halide in refluxing acetic acid (X = Cl and Br) or dichloromethane (X = I; Scheme 1). They form orange air-stable solids, insoluble in all common solvents except those with strongly donating properties. In the ^{1}H-NMR spectra, in dimethyl sulfoxide-d_6 solutions, relatively broad resonances of cyclopentadienyl (Cp) and phenyl hydrogen atoms in the range δ_H 4.15–4.75 and δ_H 7.45–7.75, respectively and a broad singlet at δ_H 12.2–12.4 for the carboxyl protons were observed (Table 1). The signals in the ^{31}P-NMR spectra are very broad ($\Delta\nu_{1/2}$ 200–950 Hz) so that the coupling constants $^1J_{HgP}$ could not be determined. Such a signal broadening most likely reflects an equilibrium between the complex, its solvolytic products and the free ligand:

$$HgX_2(Hdpf)_2 + S \rightleftarrows HgX_2(Hdpf)S_n + Hdpf \rightleftarrows HgX_2S_m + 2Hdpf;\ S = \text{solvent}$$

which may be further complicated for **2a**–**c** by cleavage of the dimers. The temperature dependence of these equilibria was not followed due to decomposition accompanied by darkening of the solutions on prolonged standing. Electrochemical behavior of the complexes in acetonitrile also indicates the presence of non-coordinated ligand (see below). Similar dissociation has already been reported for bis(phosphine)dihalido mercury(II) complexes [17], even in much less donating solvents such as dichloromethane [18]. The presence of non-coordinated ligand in the solid samples of **1a**–**c** and **2a**–**c** can be, however, excluded on the basis of the analytical data. The IR spectra of the complexes are all similar and, in general, exhibit only features due to the organometallic ligand; one of the most prominent being composed $\nu_{C=O}$ bands of the non-coordinated carboxyl group at 1670–1720 cm^{-1}.

2.2. Electrochemistry

Due to solvolytic equilibria, the electrochemical response of all the complexes is to be analyzed as the superposition of that of free Hdpf and of the product of solvolysis (Scheme 2). The cyclovoltammograms display patterns typical of an ECE process. First, one-electron oxidation of Hdpf affords the corresponding ferrocenium $[Hdpf]^+$ (E_{pa1} 0.37 V vs. ferrocene/ferrocenium), which immediately undergoes an intramolecular elec-

Table 1
^{1}H- and ^{31}P{^{1}H}-NMR data [a] for mercury(II) complexes **1a**–**c** and **2a**–**c**

Complex	δ_H			δ_P [d]
	Cp-protons	P*Ph*$_2$ [b]	CO_2H [c]	
1a	4.38 (s, 2H), 4.45 (s, 2H), 4.52 (s, 4H)	7.46–7.53 (6H), 7.54–7.64 (4H)	12.2	21.2
1b	4.26 (at, 2H), 4.41 (s, 2H), 4.51 (aq, 4H)	7.46–7.60 (10H)	12.3	14.6
1c	4.17 (s, 2H), 4.43 (s, 2H), 4.49 (s, 2H), 4.52 (s, 2H)	7.44–7.59 (10H)	12.3	0.7
2a	4.51 (s, 2H), 4.66 (s, 2H), 4.69 (s, 4H)	7.55–7.73 (10H)	12.4	29.8
2b	4.46 (s, 2H), 4.65 (at, 2H), 4.69 (s, 4H)	7.56–7.71 (10H)	12.4	26.0
2c	4.38 (s, 2H), 4.63 (s, 2H), 4.65 (s, 4H)	7.53–7.69 (10H)	12.4	15.5

[a] In dimethyl sulfoxide-d_6 at 298.0 K; s, singlet; at, apparent triplet; aq, apparent quartet; all signals broad.
[b] Multiplet.
[c] Broad singlet, 1H.
[d] Very broad signal; ^{199}Hg satelites not identified. Compare to δ_P −18.3 for free Hdpf under the same conditions.

$$[HgX_2(Hdpf)2] + solv \rightleftharpoons [HgX_2(Hdpf)(solv)_n] + Hdpf \rightleftharpoons [HgX_2(solv)_m] + 2\ Hdpf \quad (solvolysis)$$

$$Hdpf \longrightarrow [Hdpf]^+ + e^- \quad (1st\ wave,\ oxidation)$$

$$[Hdpf]^+ \xrightarrow{[O]} HdpfO \quad (consecutive\ chemical\ reaction)$$

$$HdpfO \rightleftharpoons [HdpfO]^+ + e^- \quad (2nd\ wave,\ reversible)$$

$$[HgX_2(Hdpf)(solv)_n] \longrightarrow [HgX_2(Hdpf)(solv)_n]^+ + e^- \quad (3rd\ wave,\ oxidation)$$

Scheme 2. Electrochemical behavior of Hg(II)–Hdpf complexes.

tron transfer from P(III) to Fe(III), producing very unstable species with formally tetravalent phosphorus {P(IV)Fe(II)} [19]. However, this step is instantly followed by fast chemical reactions of the species with traces of oxygen and water in the solvent [20] producing phosphine oxide (HdpfO) [13]. Therefore, almost no reduction counterpeak of $[Hdpf]^+$ is observed (Fig. 1). The product of the subsequent chemical reactions, HdpfO, exhibits a reversible one-electron ferrocene–ferrocenium wave ($HdpfO \rightleftarrows [HdpfO]^+$, E_2 ca. 0.5 V vs. ferrocene). Only the peaks with E_{pa} above 0.7 V (E_3) belong to the ferrocene-based oxidation in partly solvolyzed mercury–Hdpf complexes (Table 2). A potential shift of E_3 by ca. +200 mV observed on changing acetonitrile for the 4:1 (v/v) acetonitrile-*N*,*N*-dimethylformamide mixture indicates that the solvents are probably involved in coordination to mercury. The corresponding reduction peaks are not resolved enough to provide E_{pc} values. Moreover, the amplitude of these peaks is further lowered as the result of dissociation of the oxidized complexes. An analogous behavior has been reported for complexes of *P*,*P*′-chelating 1,1′-bis(diphenylphosphino)ferrocene [19] and other *P*-coordinated ferrocenylphosphines [21,22] with d^{10} metals. Among the studied complexes, the iodo complexes are the most stable towards solvolysis as follows from the relative heights of the peaks at the E_3 potential. Since the solvolytic equilibria are fast, free Hdpf is produced by solvolysis in the neighborhood of the electrode during the course of the electrochemical oxidation. However, as it is instantly consumed by the oxidation and subsequent chemical transformation into HdpfO, the corresponding wave gains in height on the cyclovoltammograms and the relative heights of the peaks (i.e. **1** versus **3**) does not correspond to the true equilibrium concentrations of the non-coordinated ligand and the mercury(II) species.

2.3. Crystal structures of *1b* and *2b*·4CH_3CO_2H

Search in the Cambridge Crystallographic Data Centre [23] revealed that ferrocene–mercury compounds whose crystal structures are known are represented only

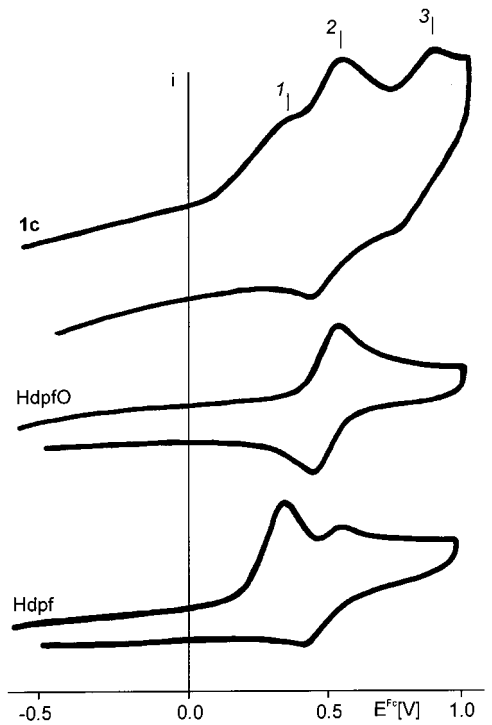

Fig. 1. Cyclovoltammograms of Hdpf, its phosphine oxide HdpfO and complex $[HgI_2(Hdpf\text{-}P)_2]$ (**1c**) in 0.05 mol l^{-1} $[Bu_4N][PF_6]$/acetonitrile at glassy carbon disc electrode (scan rate 250 mV s^{-1}). Potentials are in Volt versus ferrocene/ferrocenium.

Table 2
Cyclic voltammetric data [a] for complexes **1a–c** and **2a–c**

Compound	1st wave	2nd wave		3rd wave
	E_{pa} (V)	E_{pa} (V)	E_{pc} (V)	E_{pa} (V)
Hdpf	0.36			
HdpfO		0.54	0.45	
1a	0.36	0.56	0.46	0.82
1b	0.37	0.55	0.46	0.83
1c	0.37	0.54	0.46	0.85
2a	0.36	0.55	0.46	0.73
2b	0.37	0.55	0.44	0.77
2c	0.36	0.53	0.43	0.83

[a] See Section 3 for conditions.

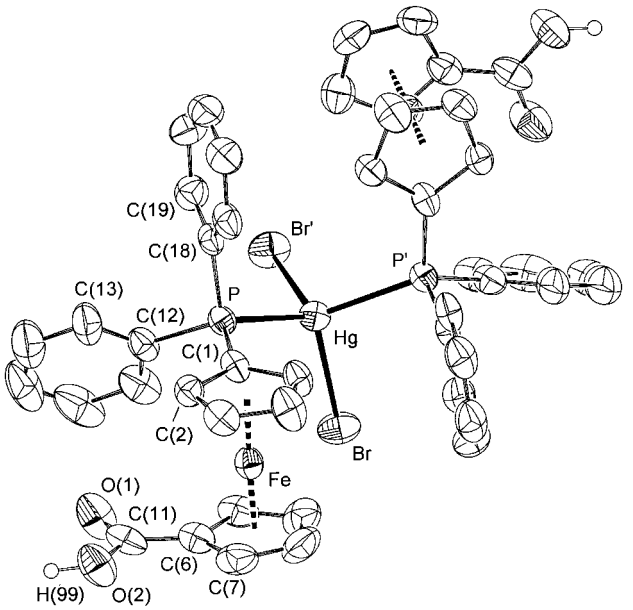

Fig. 2. Perspective view of **1b** showing thermal ellipsoids at 50% probability level and the atom numbering scheme. For clarity, hydrogen atoms were omitted and only two atoms of each ring were labelled.

by several Cp-ring metalated ferrocenes, the adduct $FcH{\cdot}7HgI_2$ [24] and by two mercury(II) complexes with *S*- [25] and *Se*,*N*-ferrocene donors [26]. Very recently, the crystal structure of the closely related solvate dichloro-(1,1′-bis(diphenylphosphino)ferrocene-*P*,*P*′)-mercury(II)-methanol (1/1), $[\{Fe(\eta^5\text{-}C_5H_4PPh_2)_2\text{-}P,P'\}HgCl_2]{\cdot}MeOH$ was reported [27]. Surprisingly, there are only five crystallographically characterized complexes of the $[HgBr_2P_2]$ and $[Hg_2Br_4P_2]$ type (P = monodentate phosphine) reported so far. The structures of the complexes **1b** (Fig. 2, Table 3) and $\mathbf{2b}{\cdot}4CH_3CO_2H$ (Fig. 3, Table 4) are the first crystallographically characterized compounds of divalent mercury with monodentate *P*-ligands derived from the ferrocene skeleton. Complex **1b** crystallizes with four molecules per monoclinic unit cell (space group $C2/c$) with the mercury atom residing on the crystallographic two-fold axis. Therefore, only one half of the molecule is symmetrically independent. The compound is a neutral complex with two *P*-coordinated ligand molecules and two bromo ligands forming a distorted tetrahedral coordination polyhedron. As a result of the steric demands of the phosphine ligand, the PHgP angle is more opened in comparison with the remaining angles around the metal centre. The metal ligand distances Hg–P 2.529(2) and Hg–Br 2.6200(7) Å in **1b** are comparable to those found for the related Hg_2BrL_2 complex where L is 1-phenyldibenzophosphole [28], whereas shorter Hg–P and longer Hg–Br distances were reported for a complex with $P(CH_2CH_2CN)_3$ as the *P*-donor (both by ca. 0.1 Å) [29]. The carboxyl group of the ligand does not participate in coordination to mercury(II). Instead, it is involved in hydrogen bonding to the carboxyl group of the neighboring ligand at the O···O distances of 2.647(8) Å, resulting in infinite chains running in the crystallographic *ab* plane. No further intermolecular contacts were found in the structure except for those at the van der Waals radii level.

Although complex **2b**, prepared as mentioned above, is unsolvated X-ray quality crystals were obtained only for the acetic acid solvate $\mathbf{2b}{\cdot}4CH_3CO_2H$. This complex forms a centrosymmetric dimer located at the crystallographic symmetry centre. One molecule of the solvating acetic acid is connected to the ligand carboxyl group by a double hydrogen bridge [O···O 2.638(9) and 2.654(9) Å]. The second is joined by a centrosymmetric two-fold hydrogen bond to its centrosymmetric counterpartner $[(CH_3CO_2H)_2$, O···O 2.661(9) Å]. The structure is essentially molecular since the uncoordinated carboxyl group of the ligand is blocked by hydrogen bonding to acetic acid and no further intermolecular contacts were identified in the structure. The coordination polyhedron of complex **2b** can be described in terms of two edge-

Table 3
Selected bond lengths (Å), bond angles and dihedral angles of least-squares planes (°) for **1b** with estimated S.D. in parentheses [a,b]

Ligand (average values)			
Fe–C(Cp)	2.04(1; $n=10$)		
C–C(Cp)	1.42(2; $n=10$)	C–C–C(Cp)	108(1; $n=10$)
C–C(Ph)	1.38(1; $n=12$)	C–C–C(Ph)	120.0(6; $n=12$)
Coordination and P-ligand geometry			
Hg–P	2.529(2)	P–Hg–P^{i}	118.71(7)
Hg–Br	2.6200(7)	P–Hg–Br	113.31(4)
P–C(01)	1.785(6)	P^{i}–Hg–Br	104.23(4)
P–C(18)	1.811(6)	Br–Hg–Br^{i}	102.01(4)
P–C(12)	1.819(6)	C(01)–P–C(12)	107.1(3)
Hg–Fe	4.776(1)	C(01)–P–C(18)	103.8(3)
C(12)–P–C(18)	105.0(3)		
H-Bonded carboxyl groups			
C(06)–C(11)	1.451(10)	O(1)–C(11)–O(2)	122.0(7)
O(1)–C(11)	1.255(9)	C(11)–O(2)–H(99)	121(5)
O(2)–C(11)	1.279(8)	O(1)–C(11)–C(06)	120.5(6)
O(2)–H(99)	0.96(9)	O(2)–C(11)–C(06)	117.4(7)
O(1)···O(2^{ii})	2.647(8)	O(2)–H(99)···O(1^{ii})	167(8)
O(1)···H(99^{ii})	1.70(9)		
Dihedral angles of least-squares planes [c]			
Cp1 vs. Cp2	2.9(7)	Cp1 vs. Ph1	65.0(2)
Cp2 vs. CO_2H	4(1)	Cp1 vs. Ph2	86.9(3)
		Ph1 vs. Ph2	76.3(2)

[a] Symmetry codes: (i) $-x$, y, $1/2-z$; (ii) $1/2-x$, $1/2-y$, $-z$.
[b] Arithmetic mean of n values.
[c] Planes are defined as follows: Cp1: C(01), C(02), C(03), C(04), C(05); Cp2: C(06), C(07), C(08), C(09), C(10); CO_2H: C(11), O(1), O(2); Ph1: C(12), C(13), C(14), C(15), C(16), C(17); Ph2: C(18), C(19), C(20), C(21), C(22), C(23).

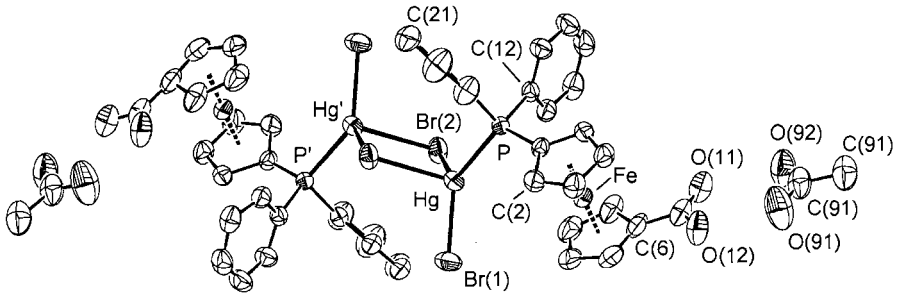

Fig. 3. Perspective view of **2b**·4CH_3CO_2H. Thermal ellipsoids are drawn at 50% probability level. The labelling scheme of the Hdpf ligand is identical to that of **1b** thus, only one carbon atom of each ring is labelled. For clarity, all hydrogen atoms and molecules of solvating acetic acid which are not involved in the hydrogen bonding to the ligand carboxyl group were omitted.

sharing distorted tetrahedra where the Br(2)–Br(2^i) edge (i: $1-x$, $-y$, $1-z$) is the shortest and the Br(1)–P edge the longest. In comparison to **1b**, the coordination polyhedron is more distorted; the bond angles vary from 90 ($Br_{bridge}HgBr_{bridge}$) to 137° ($PHgBr_{terminal}$). Similar structural features have been observed for the triphenylphosphine derivative $[Hg(PPh_3)Br_2]_2$ [30], for $[Hg\{P(CH_2CH_2CH_3)Br_2]_2$ [31], and also for the complex with the related phosphinocarboxylic ligand, (diphenylphosphino)acetic acid $[Hg(Ph_2PCH_2CO_2H)Br_2]_2$ [32]. Both Hg–P and Hg–$Br_{terminal}$ bond lengths in **2b**·4CH_3CO_2H (2.425(1) and 2.4993(7) Å, respectively) are shorter than those in **1b** by ca. 0.1 Å. The Hg–Br_{bridge} bonds 2.7545(8) and 2.7932(8) Å for Br(2) and Br(2^i), respectively, differ slightly but they are markedly longer when compared to the Hg–$Br_{terminal}$ bonds.

In both complexes the bond distances and angles within the ferrocene moiety remain almost unaffected by the coordination. The Cp-rings are almost parallel with the dihedral angles of the Cp-planes for **1b** [in square brackets for **2b**·4CH_3CO_2H] of 2.9(7)° [3.8(7)°]; the Fe–centroid distances are 1.644 [1.646] Å and 1.642 [1.651] Å for phosphinylated and carboxylated Cp-rings, respectively. The dihedral angles between the carboxyl plane and its parent Cp-ring of 4(1)° [6(2)°] indicate that no significant torsion occurs at the C(Cp)–CO_2 bond on the formation of hydrogen bonds. However, hydrogen bonding is most likely responsible for the profound conformational changes within the ferrocene moiety: while the substituents on the ferrocene frame in **1b** adopt a *syn*-eclipsed conformation characterized by the τ(P–centroid–centroid–CO_2) torsion angle of $-80.4°$ (cf. 72° for the exactly eclipsed conformation), the substituents in **2b**·4CH_3CO_2H are *anti*-eclipsed with $\tau = 134.1°$ (the ideal value is 144°).

2.4. Mössbauer spectra

The Mössbauer spectra of all the complexes consist of simple quadrupole doublets (Table 5). Due to preferred orientation of the polycrystalline samples, the doublets are asymmetric; however, the ratio of the areas of the doublet components D_{21} differ by less than 20%.

On going from ferrocene to Hdpf, a decrease of the quadropole splitting (E_Q) value by 0.09 mm s^{-1} is observed. This is the consequence of the attachement of two electron-withdrawing substituents to the ferrocene moiety because such substituents lower the overall electron density on the Cp-rings and hence, reduce the asymmetry of the electron charge distribution around the ferrocene iron atom [33]. The bonding of Hdpf as the *P*-ligand to mercury(II) leads to an increase of the back donation from the Cp-ring into the empty 3d orbitals of phosphorus [34] thus causing a further decrease of E_Q. The significantly lower magnitude of this second decrease indicates that the electronic changes during the complex formation take place predominantly at the phosphorus atom. This is in accord with the previous observation that the lone pair at the phosphorus atom in non-coordinated (diphenylphosphino)-ferrocene is not involved in bonding between the diphenylphosphino group and the ferrocene unit [35]. Accordingly, the donation of the lone pair does not affect Mössbauer parameters of the ferrocene moiety in any significant way, especially when no large contribution of the back donation to coordination bonds might be expected (d^{10} metal). In general, the higher the contribution of π-back bonding to the metal–phosphine bond, the larger decrease of E_Q is observed as manifested by the ΔE_Q values for palladium(II) and copper(I) complexes given in Table 5. The isomer shift (δ) values of **1a**–**c** and **2a**–**c** are very similar, thus reflecting the long distance of the iron atom from the coordination site and also only marginal changes of coordination geometry between the complexes [36].

3. Experimental

3.1. General considerations

All solvents were purified using standard procedures. The ligand was syntesized as reported previously [13]. ^{1}H-NMR (399.95 MHz) and ^{31}P{^{1}H}-NMR (161.90 MHz) spectra were measured on a Varian Unity Inova 400 spectrometer with internal tetramethylsilane (^{1}H) and external 85% aqueous H_3PO_4 (^{31}P) as standards. All NMR spectra were recorded at 298.0(1) K in dimethyl sulfoxide-d_6 solutions. Zero-field ^{57}Fe transmission Mössbauer spectra of polycrystalline samples were measured in the conventional constant acceleration mode using ^{57}Co deposited in the Cr matrix as the γ-ray source. The measurements were carried out at room temperature (r.t.) with 500 channels for the velocity range of $\langle -4.8; 4.8\rangle$ mm s^{-1}. The Mössbauer parameters were evaluated by a curve fitting procedure (Lorentzian line shape); α-Fe was used as the velocity-scale calibrant and as the reference for the isomer shift values.

Electrochemical experiments were performed at 25°C on a multipurpose polarograph GWP 673 (ZWG Berlin, Germany) using inert-gas (argon) flow three-electrode cell (standard Metrohm type) equipped with a glassy carbon rotating disc working electrode (2 mm diameter), a platinum foil auxiliary electrode and SCE as the reference electrode. Cyclic voltammograms were recorded at the scan rate of 250 mV s^{-1} on the stationary electrode, polarograms were measured on the rotating electrode (500 min^{-1}) with the scan rate of 0.5 V min^{-1}. Potentials are given in volts relative to the redox potential of internal ferrocene/ferrocenium. The concentrations of the compounds were as follows: saturated (**1a**–**c**, **2a**–**c**) or 4 mmol l^{-1} (Hdpf, HdpfO) in 0.05 mol l^{-1} solution of [Bu_4N][PF_6] in acetonitrile and 4 mmol l^{-1} (all compounds) in a solution of the same supporting electrolyte (0.05 mol l^{-1}) in acetonitrile-*N*,*N*-dimethylformamide 4:1 (v/v). Acetonitrile (Fluka, puriss.) was used as received. *N*,*N*-Dimethylformamide was dried by azeotropic distillation with water and benzene followed by fractionation in vacuo.

Table 4
Selected bond lengths (Å), bond angles and dihedral angles of least-squares planes (°) for **2b**·4CH_3CO_2H with estimated S.D. in parentheses [a]

Ligand (average values) [b]			
Fe–C(Cp)	2.04(1; $n=10$)		
C–C(Cp)	1.42(1; $n=10$)	C–C–C(Cp)	108.0(5; $n=10$)
C–C(Ph)	1.377(9; $n=12$)	C–C–C(Ph)	120.0(9; $n=12$)
Coordination and P-ligand geometry			
Hg–P	2.425(1)	P–Hg–Br(1)	137.44(4)
Hg–Br(1)	2.4993(7)	P–Hg–Br(2)	105.35(4)
Hg–Br(2)	2.7545(8)	P–Hg–Br(2^i)	104.22(4)
Hg–Br(2^i)	2.7932(8)	Br(1)–Hg–Br(2)	107.68(3)
P–C(01)	1.786(5)	Br(1)–Hg–Br(2^i)	101.68(3)
P–C(12)	1.812(6)	Br(2)–Hg–Br(2^i)	90.32(2)
P–C(18)	1.811(6)	Hg–Br(2)–Hg^i	89.68(2)
Hg–Fe	4.409(1)	C(01)–P–C(12)	105.0(3)
		C(01)–P–C(18)	106.7(3)
		C(12)–P–C(18)	107.5(3)
H-Bonded carboxyl groups and solvating acetic acid			
O(12)…O(91)	2.638(9)	O(92)–H(91)…O(11)	158(8)
O(92)…O(11)	2.654(9)	O(92)–H(91)…O(11)	158(8)
O(82)…O(81^{ii})	2.661(9)	O(82)–H(81)…O(81^{ii})	170(1)
C(06)–C(11)	1.45(1)	O(11)–C(11)–O(12)	123.2(7)
O(11)–C(11)	1.25(1)	O(11)–C(11)–C(06)	119.5(7)
O(12)–C(11)	1.27(1)	O(12)–C(11)–C(06)	117.3(8)
O(12)–H(90)	0.76(8)		
C(81)–C(82)	1.49(1)	O(81)–C(81)–O(82)	123.2(8)
O(81)–C(81)	1.220(9)	O(81)–C(81)–C(82)	120.9(8)
O(82)–C(81)	1.28(1)	O(82)–C(81)–C(82)	115.9(9)
O(82)–H(81)	0.72(9)		
C(91)–C(92)	1.47(1)	O(92)–C(91)–O(91)	121.7(8)
O(91)–C(91)	1.26(1)	O(92)–C(91)–C(92)	119(1)
O(92)–C(91)	1.24(1)	O(91)–C(91)–C(92)	120(1)
O(92)–H(91)	0.83(8)		
Dihedral angles of least-squares planes [c]			
Cp1 vs. Cp2	3.8(7)	Cp1 vs. Ph1	82.2(2)
Cp2 vs. CO_2H	6(2)	Cp1 vs. Ph2	70.1(3)
Ph1 vs. Ph2	72.6(2)		

[a] Symmetry codes: (i) $1-x, -y, 1-z$; (ii) $1-x, -y, -z$.
[b] Arithmetic mean of n values.
[c] Planes are defined as follows: Cp1: C(01), C(02), C(03), C(04), C(05); Cp2: C(06), C(07), C(08), C(09), C(10); CO_2H: C(11), O(1), O(2); Ph1: C(12), C(13), C(14), C(15), C(16), C(17); Ph2: C(18), C(19), C(20), C(21), C(22), C(23).

Table 5
^{57}Fe Mössbauer parameters for **1a**–**c** and **2a**–**c** given relative to the Fe metal at room temperature

Compound	δ (mm s^{-1})	E_Q (mm s^{-1})	D_{21} [a]
Ferrocene	0.45	2.39	1.10
Hdpf	0.45	2.30	0.93
1a	0.43	2.23	0.99
1b	0.43	2.23	0.83
1c	0.44	2.24	0.93
2a	0.43	2.20	1.13
2b	0.44	2.21	0.97
2c	0.43	2.22	1.12
trans–[Pd(Hdpf-*P*)$_2$Cl$_2$] [b]	0.42	2.22	1.22
[Cu_4I_4(Hdpf-*P*)$_4$]·2CH_3CO_2H [c]	0.44	2.26	1.03

[a] D_{21} is the ratio of the areas of the doublet components due to $m_l \pm 3/2 \leftarrow \pm 1/2$ and $\pm 1/2 \leftarrow \pm 1/2$ transitions, where m_l is the magnetic quantum number.
[b] Sample from Ref. [14].
[c] Sample from Ref. [15].

Table 6
Crystallographic data for **1b** and **2b**·4CH_3CO_2H

Complex	**1b**	**2b**·4CH_3CO_2H
Formula	$C_{46}H_{38}Br_2Fe_2HgO_4P_2$	$C_{54}H_{54}Br_4Fe_2Hg_2O_{12}P_2$
M	594.41	894.72
Crystal system	Monoclinic	Triclinic
Space group	$C2/c$ (no. 15)	$P\bar{1}$ (no. 2)
a (Å)	19.453(1)	9.442(1)
b (Å)	13.704(1)	11.7101(9)
c (Å)	17.929(2)	14.806(1)
α (°)		109.692(7)
β (°)	114.953(7)	92.494(9)
γ (°)		101.883(7)
V (Å^3)	4333.4(6)	1496.9(2)
Z	4	1
$D_{calc.}$ (g ml^{-1})	1.822	1.985
$F(000)$	2312	856
Crystal size (mm^3)	$0.13\times0.15\times0.18$	$0.46\times0.96\times1.0$
Crystal description	Orange prism	Orange prism
μ (mm^{-1})	6.16	8.37
T_{min}; T_{max} [a]	0.373; 0.517	0.116; 0.403
2θ range (°)	3.8–50.0	2.9–50.0
hkl range	$-23\rightarrow20$, $0\rightarrow16$, $0\rightarrow21$	$-11\rightarrow11$, $-13\rightarrow12$, $0\rightarrow17$
No. of diffractions collected; $R(\sigma)$ [b] (%)	3922; 5.0	5259; 3.0
No. of diffractions unique	3797	5259
No. of observed diffractions; $F_o\geq4\sigma(F_o)$	2905	4238
Standard diffractions	Three monitored every hour	
Variation in standards (%)	3	14
Weighting scheme: w_1, w_2 [c]	0.0544, 1.4384	0.0667, 0.4671
No. of parameters	262	379
R_{all} (F), R_{obs} (F) [b] (%)	6.9, 3.7	5.5, 3.5
wR_{all} (F^2), wR_{obs} (F^2) [b] (%)	9.5, 8.4	9.8, 9.0
GOF_{all} [a]	1.04	1.04
$(\Delta/\sigma)_{max}$	0.000	0.000
$\Delta\rho$ (e Å^{-3})	1.76, −1.32	2.11, −1.10

[a] Transmission coefficients (see Section 3).

[b] $R(F)=\Sigma(\|F_o\|-\|F_c\|)/\Sigma|F_o|$, $wR(F^2)=[\Sigma w(F_o^2-F_c^2)^2/w(F_o^2)^2]^{1/2}$, $GOF=[\Sigma(w(F_o^2-F_c^2)^2)/(N_{diffrs}-N_{params})]^{1/2}$, $R(\sigma)=\Sigma\sigma(F_o^2)/\Sigma F_o^2$.

[c] Weighting scheme: $w=[\sigma^2(F_o^2)+w_1P^2+w_2P]^{-1}$; $P=[max(F_o^2)+2F_c^2]/3$.

3.2. Syntheses

3.2.1. [$HgCl_2$(Hdpf-P)$_2$] (**1a**)

A solution of $HgCl_2$ (67.5 mg, 0.25 mmol) in acetone (2 ml) was added to a solution of Hdpf (207.4 mg, 0.50 mmol) in hot acetic acid (5 ml). The mixture was cooled to r.t. and allowed to stand at 0°C for several days. The resulting precipitate was filtered off, washed with diethyl ether (5 × 5 ml) and dried at 100°C for 2 h. Yield: 263.1 mg (96%) of an orange microcrystalline solid. Anal. Found: C, 50.10; H, 3.32. $C_{46}H_{38}Cl_2Fe_2HgO_4P_2$ Calc. C, 50.23; H, 3.48%. IR, $\tilde{\nu}$/cm^{-1}: 1720 vs, 1678 vs, 1287 m, 1230 m, 1193 m, 1172 m, 1134 m, Fc 1104 m, 1030 m, 837 w (composite), 754 m, 693 m, 461–540 m (composite).

3.2.2. [$HgCl(\mu$-$Cl)$(Hdpf-P)]$_2$ (**2a**)

Following the same procedure as for the preparation of **1a**, $HgCl_2$ (67.4 mg, 0.25 mmol) and Hdpf (103.8 mg, 0.25 mmol) provided **2a** as orange crystals (168.2 mg, 98%). Anal. Found: C, 40.43; H, 2.58. $C_{46}H_{38}Cl_4Fe_2Hg_2O_4P_2$ Calc. C, 40.29; H, 2.79%. IR, $\tilde{\nu}$/cm^{-1}: 1719 vs, 1291 s, 1167 s (composite), 1102 m, 1031 s, 840 m, (composite), 749 s, 693 s, 471–564 s (composite).

3.2.3. [$HgBr_2$(Hdpf-P)]$_2$ (**1b**)

Similarly to **1a**, $HgBr_2$ (90.2 mg, 0.25 mmol) and Hdpf (207.9 mg, 0.50 mmol) gave **1b** as an orange crystalline solid (266.8 mg, 90%). Anal. Found: C, 46.49; H, 2.97. $C_{46}H_{38}Br_2Fe_2HgO_4P_2$ Calc. C, 46.47; H, 3.22%. IR, $\tilde{\nu}$/cm^{-1}: 1676 vs, 1287 s, 1166 s, 1161 s, 1134 m, 1098 m, 1030 m, 930 w (broad), 840 m (composite), 743 s, 691 s, 481–508 s (composite).

The crystal used for X-ray analysis was selected form the reaction batch before washing with diethyl ether since the washing causes partial crystal disintegration.

3.2.4. [$HgBr(\mu$-$Br)$(Hdpf-P)]$_2$ (**2b**)

Starting from $HgBr_2$ (90.3 mg, 0.25 mmol) and Hdpf (104.8 mg, 0.25 mmol), the above mentioned procedure provided **2b** as orange crystals (190.5 mg, 98%). Anal. Found: C, 36.69; H, 2.50. $C_{46}H_{38}Br_4Fe_2Hg_2O_4P_2$ Calc. C, 35.66; H, 2.47%. IR, $\tilde{\nu}$/cm^{-1}: 1710 vs, 1693 vs, 1674 vs, 1297 s, 1168 s, 1098 m, 1033 m, 844 m (composite), 748 s, 689 m, 469–515 m (composite).

The clear crystals become opaque on washing with diethyl ether and give only very broad diffraction spots. Crystals suitable for X-ray structural analysis were obtained as follows: a solution of $HgBr_2$ (1.8 mg, 5.0 μmol) in hot acetic acid (1 ml) was added to a solution of Hdpf (2.2 mg, 5.3 μmol) in hot toluene (1 ml). The clear solution was boiled briefly and left to stand at r.t. The crystals which formed after several weeks were isolated by suction and dried in air. Unlike the product prepared in the larger scale as described above, the crystals contain four molecules of solvating acetic acid per one molecule of the complex (confirmed by ^{1}H-NMR and IR spectra; **2b** · 4CH_3CO_2H).

3.2.5. [HgI_2(Hdpf-P)$_2$] (**1c**)

A solution of Hdpf (207.6 mg, 0.50 mmol) in dichloromethane (5 ml) was added to a stirred suspension of HgI_2 (113.4 mg, 0.25 mmol) in the same solvent

Table 7
Atomic coordinates ($\times 10^4$) and equivalent isotropic displacement parameters ($Å^2 \times 10^3$) for **1b** [a]

Atom	x/a	y/b	z/c	U_{eq}
Hg	0	2871(1)	2500	40(1)
Br	1121(1)	4074(1)	3286(1)	61(1)
Fe	2068(1)	1244(1)	2259(1)	40(1)
P	161(1)	1931(1)	1370(1)	36(1)
O(1)	2183(4)	2972(4)	688(4)	77(2)
O(2)	3037(3)	1818(4)	865(4)	72(2)
C(01)	921(4)	1071(4)	1693(4)	39(1)
C(02)	1269(3)	628(4)	1225(4)	41(1)
C(03)	1781(4)	−88(5)	1706(4)	49(2)
C(04)	1751(5)	−117(5)	2479(5)	61(2)
C(05)	1233(4)	611(5)	2486(4)	45(2)
C(06)	2731(4)	2165(5)	1963(4)	51(2)
C(07)	3189(4)	1444(6)	2516(5)	64(2)
C(08)	3067(4)	1514(7)	3233(5)	72(2)
C(09)	2563(5)	2274(6)	3149(5)	68(2)
C(10)	2334(4)	2684(5)	2371(5)	55(2)
C(11)	2641(4)	2339(5	1129(5)	54(2)
C(12)	215(4)	2643(5)	540(4)	46(2)
C(13)	−8(4)	2239(6)	−233(4)	66(2)
C(14)	63(5)	2767(9)	−849(6)	88(3)
C(15)	361(6)	3695(9)	−699(7)	93(4)
C(16)	574(5)	4098(7)	57(8)	91(3)
C(17)	498(4)	3581(6)	690(5)	67(2)
C(18)	−680(4)	1183(5)	881(4)	40(1)
C(19)	−1372(4)	1654(6)	469(4)	54(2)
C(20)	−2038(4)	1123(6)	152(5)	63(2)
C(21)	−2027(5)	140(7)	261(5)	66(2)
C(22)	−1355(4)	−339(6)	653(4)	58(2)
C(23)	−673(4)	182(5)	972(4)	51(2)

[a] Estimated S.D. in the last significant figure are given in parentheses.

(5 ml). The mercury(II) salt dissolves and, simultaneously, an orange powder is precipitated. The mixture was stirred at r.t. for 1 h, then cooled to 0°C overnight. Filtration, washing with diethyl ether (5 × 5 ml) and drying at 100°C for 2 h yielded **1c** as an orange microcrystalline solid (291.8 mg, 91%). Anal. Found: C, 43.04; H, 2.84. $C_{46}H_{38}Fe_2HgI_2O_4P_2$ Calc. C, 43.07; H, 2.99%. IR, $\tilde{\nu}/cm^{-1}$: 1674 vs, 1286 s, 1162 s, 1098 m, 1029 m, 840 m (composite), 743 m, 692 m, 468–563 m (composite).

3.2.6. [HgI(μ-I)(Hdpf-P)]$_2$ (2c)

Following the procedure for the preparation of **1c**, HgI_2 (113.9 mg, 0.25 mmol) and Hdpf (114.5 mg, 0.28 mmol) gave **2c** as an orange–yellow solid (205.7 mg, 95%). Anal. Found: C, 31.80; H, 2.00. $C_{46}H_{38}Fe_2Hg_2I_4O_4P_2$ Calc. C, 31.80; H, 2.20%. IR, $\tilde{\nu}/cm^{-1}$: 1673 vs, 1294 s, 1167 s, 1103 m, 1033 m, 1027 m, 840 m (composite), 737 s, 688 m, 467–564 s (composite).

3.3. X-ray crystallography

Single crystals of **1b** and **2b**·4CH_3CO_2H suitable for X-ray analysis were grown as described above. All diffraction data were measured at 296(2) K on an Enraf–Nonius CAD 4-MACH III diffractometer using graphite-monochromated Mo–K_α radiation (λ = 0.71073 Å) and the $\theta - 2\theta$ scan. The intensities were corrected for Lorentz-polarization effects and analytically corrected for absorption after indexation of the crystal faces (AGNOSTIC [37] transmission coefficients T_{min} and T_{max} given in Table 2). The cell parameters were refined by least-squares from 25 automatically centered diffractions with $13 \leq \theta \leq 14°$ and $14 \leq \theta \leq 15°$ for **1b** and **2b**·4CH_3CO_2H, respectively.

The structures were solved by combination of direct and heavy-atom methods (SHELXL86 [38]) and refined by full-matrix least-squares on F^2 (SHELXL93 [39]). All non-hydrogen atoms were refined anisotropically. All

Table 8
Atomic coordinates ($\times 10^4$) and equivalent isotropic displacement parameters ($Å^2 \times 10^3$) for **2b** · 4CH_3CO_2H [a]

Atom	x/a	y/b	z/c	U_{eq}
Hg	6596(1)	76(1)	4207(1)	47(1)
Br(1)	6968(1)	−2054(1)	3332(1)	76(1)
Br(2)	3660(1)	−33(1)	3932(1)	53(1)
Fe	9955(1)	1502(1)	2625(1)	43(1)
P	7812(2)	2217(1)	4467(1)	33(1)
O(11)	9969(6)	2640(6)	487(4)	76(2)
O(12)	12026(7)	2074(8)	690(5)	82(2)
C(01)	9504(6)	2401(5)	3978(4)	34(1)
C(02)	10623(7)	1770(6)	4027(5)	48(2)
C(03)	11808(7)	2272(7)	3598(5)	54(2)
C(04)	11421(7)	3178(6)	3285(5)	49(2)
C(05)	9998(6)	3268(5)	3507(4)	40(1)
C(06)	9953(8)	1126(7)	1186(5)	61(2)
C(07)	8497(8)	986(8)	1416(5)	66(2)
C(08)	8225(9)	64(7)	1842(6)	71(2)
C(09)	9494(12)	−390(7)	1868(6)	82(3)
C(10)	10567(10)	263(7)	1470(6)	75(2)
C(11)	10683(8)	2008(8)	770(5)	60(2)
C(12)	6749(6)	3044(5)	3976(4)	36(1)
C(13)	5860(7)	2421(6)	3106(5)	45(1)
C(14)	5170(7)	3072(7)	2680(5)	56(2)
C(15)	5362(8)	4347(7)	3119(6)	59(2)
C(16)	6227(8)	4954(6)	3979(6)	58(2)
C(17)	6936(7)	4314(6)	4415(5)	47(2)
C(18)	8212(6)	3051(5)	5758(4)	39(1)
C(19)	7066(8)	3233(6)	6296(5)	51(2)
C(20)	7329(10)	3780(7)	7298(5)	64(2)
C(21)	8719(11)	4105(8)	7758(6)	73(2)
C(22)	9843(11)	3917(10)	7203(6)	88(3)
C(23)	9607(8)	3392(8)	6217(6)	65(2)
O(81)	5661(8)	−13(6)	−1031(4)	87(2)
O(82)	5373(10)	1614(7)	165(5)	96(2)
C(81)	5784(9)	1109(8)	−655(6)	65(2)
C(82)	6407(20)	1975(11)	−1157(9)	102(4)
O(91)	13273(7)	3558(8)	−197(7)	118(3)
O(92)	11249(8)	4101(8)	−423(6)	99(2)
C(91)	12563(10)	4186(8)	−499(6)	71(2)
C(92)	13279(14)	4989(12)	−1004(9)	90(4)

[a] Estimated S.D. in the last significant figure are given in parentheses.

aromatic hydrogens were included in theoretical positions with C–H 0.93 Å and assigned $U_{iso}(H) = 1.2\ U_{eq}(C)$, those of carboxyl and methyl groups (*H*dpf, CH_3CO_2H) were found on the difference electron density map and isotropically refined. Further relevant crystal data, details of intensity measurements and structure solution is summarized in Table 6. The final positional parameters of non-hydrogen atoms along with their equivalent isotropic displacements parameters are given in Tables 7 and 8.

Acknowledgements

This work was supported by grants from the Grant Agency of Charles University (no. 206/1996) and the Grant Agency of the Czech Republic (no. 203/96/0948 and 203/96/0111).

References

[1] A. Togni, T. Hayashi (Eds.), Ferrocenes, VCH, Weinheim, 1995.
[2] O. Lavastre, J. Plass, P. Bachmann, S. Guesmi, C. Moinet, P.H. Dixneuf, Organometallics 16 (1997) 184.
[3] T.M. Miller, K.J. Ahmed, M. Wrighton, Inorg. Chem. 28 (1989) 2347.
[4] P. Štěpnička, R. Gyepes, O. Lavastre, P.H. Dixneuf, Organometallics 16 (1997) 5089.
[5] G. Marr, T. Hunt, J. Chem. Soc. C (1969) 1070.
[6] M. Tsukazaki, M. Tinkl, A. Roglans, B.J. Chappel, N.J. Taylor, V. Snieckus, J. Am. Chem. Soc. 118 (1996) 685.
[7] T. Hayashi, T. Mise, M. Fukushima, M. Kagotani, N. Nagashima, Y. Hamada, A. Matsumoto, S. Kawakami, M. Konishi, K. Yamamoto, M. Kumada, Bull. Chem. Soc. Jpn. 53 (1980) 1138.
[8] O. Riant, O. Samuel, T. Flessner, S. Taudien, H.B. Kagan, J. Org. Chem. 62 (1997) 6733.
[9] G. Iftime, C. Moreau-Bossuet, E. Manoury, G.A. Balavoine, J. Chem. Soc. Chem. Commun. (1996) 527.
[10] D. Matt, M. Huhn, J. Fischer, A. De Cian, W. Kläui, I. Tkatchenko, M.C. Bonnet, J. Chem. Soc. Dalton Trans. (1993) 1173.
[11] A. Louati, M. Huhn, Inorg. Chem. 32 (1993) 3601.
[12] P. Braunstein, T.M.G. Carneiro, D. Matt, F. Balegroune, B. Grandjean, J. Organomet. Chem. 367 (1989) 117.
[13] J. Podlaha, P. Štěpnička, I. Císařová, J. Ludvík, Organometallics 15 (1996) 543.
[14] P. Štěpnička, J. Podlaha, R. Gyepes, M. Polášek, J. Organomet. Chem. 552 (1998) 293.
[15] P. Štěpnička, R. Gyepes, J. Podlaha, Collect. Czech. Chem. Commun. 63 (1998) 64.
[16] P. Štěpnička, I. Císařová, J. Chem. Soc. Dalton Trans. (1998) 2807.
[17] K.K. Chow, W. Levason, C.A. McAuliffe, in: C.A. McAuliffe (Ed.), Transition Metal Complexes of Phosphorus, Arsenic and Antimony Ligands, Part 2, MacMillan, London, 1973, p. 175.
[18] S.O. Grim, P.J. Lui, R.L. Keiter, Inorg. Chem. 13 (1974) 342.
[19] B. Corain, B. Longato, G. Favero, D. Ajó, G. Pilloni, U. Russo, F.R. Kreissl, Inorg. Chim. Acta 157 (1989) 259.
[20] The solvents used are very difficult to dry below 10 ppm of water content. However, such concentration of water (and oxygen) is of the same order as molar concentration of the studied compounds.
[21] C.J. McAdam, N.W. Duffy, B.H. Robinson, J. Simpson, J. Organomet. Chem. 527 (1997) 179.
[22] P. Zanello, G. Opromolla, G. Giorgi, G. Sasso, A. Togni, J. Organomet. Chem. 506 (1996) 61.
[23] Cambridge Crystallographic Data Centre (CCDC) 1998; for Ref. see: F. Allen, O. Kennard, Chem. Des. Autom. News 8 (1993) 1 and 31.
[24] J. Votinský, L. Beneš, J. Klikorka, J. Kalousová, J. Horák, P. Losták, J. Appl. Crystallogr. 17 (1984) 363.
[25] T. Kawamoto, Y. Kushi, J. Chem. Soc. Dalton Trans. (1992) 3137.
[26] R. Kaur, H.B. Singh, R.P. Patel, S.K. Kulshreshtha, J. Chem. Soc. Dalton Trans. (1996) 461.
[27] J. McGinley, V. McKee, C.J. McKenzie, Acta Crystallogr. Sect. C (1998) 345.
[28] Code WEBZOS in CCDC [23]; original Ref.: G.A. Bowmaker, H.J. Clase, N.W. Alcock, J.M. Kessler, J.H. Nelson, J.S. Frye, Inorg. Chim. Acta 210 (1993) 107.
[29] Structure CIZNII in the CCDC [23]; original Ref.: N.A. Bell, M. Goldstein, L.A. March, I.W. Nowell, J. Chem. Soc. Dalton Trans. (1984) 1621.
[30] Structure WEBZUY in the CCDC [23]; original Ref. [28].
[31] Structure VAXGEG in the CCDC [23]; original Ref.: N.A. Bell, L.A. March, I.W. Nowell, Inorg. Chim. Acta 162 (1989) 57.
[32] J. Podlahová, B. Kratochvíl, J. Loub, H. Paulus, Acta Crystallogr. Sect. C 42 (1986) 414.
[33] B.A. Sosinsky, Chemical Mössbauer Spectroscopy, Plenum Press, New York, 1974, pp. 1–25.
[34] A. Houlton, P.T. Bishop, P.M.G. Roberts, J. Silver, M. Herbehold, J. Organomet. Chem. 364 (1989) 381.
[35] A. Houlton, R.M.G. Roberts, J. Silver, M.G.B. Drew, J. Chem. Soc. Dalton Trans. (1990) 1543.
[36] A. Houlton, K.I. Sahd, J.R. Dilworth, J. Silver, J. Chem. Soc. Dalton Trans. (1993) 2421.
[37] D.H. Templeton, L.K., Templeton, AGNOSTIC. Program for Absortion Correction, University of California, Berkeley, 1978.
[38] G.M. Sheldrick, SHELXS86, Program for the Solution of Crystal Structures from Diffraction Data, University of Göttingen, Göttingen, 1986.
[39] G.M. Sheldrick, SHELXL93, Program for Crystal Structure Refinement from Diffraction Data, University of Göttingen, Göttingen, 1993.